Monte Carlo study of the arrival time distribution of particles in extensive air showers in the energy range 1–100 TeV

G. Battistoni [a], A. Ferrari [a], M. Carboni [b], V. Patera [c,b]

[a] *INFN Milano, 20133 Milano, Italy*
[b] *INFN Laboratori Nazionali di Frascati, 00044 Frascati (Roma), Italy*
[c] *Dipartimento di Energetica, Università "La Sapienza", 00185 Roma, Italy*

Abstract

A detailed simulation of vertical showers in atmosphere produced by primary gammas and protons, in the energy range 1–100 TeV, has been performed by means of the FLUKA Monte Carlo code, with the aim of studying the time structure of the shower front at different detector heights. It turns out that the time delay distribution can be fitted using few parameters coincident with the distribution central moments. Such parameters exhibit a smooth behaviour as a function of energy. These results can be used both for detector design and for the interpretation of the existing measurements. Differences in the time structure between gamma and proton induced showers are found and explained in terms of the nonrelativistic component of extensive air showers. © 1998 Elsevier Science B.V.

1. Introduction

Recent papers concerning calculations of Extensive Air Showers (EAS) [1] include results on time delay of particles from the shower front, in view of the comparison with existing recent measurements [2–4]. As a matter of fact, the first measurements of the structure of the EAS front were attempted by Bassi, Clark and Rossi in 1953 [5], but many other have contributed [6–12]. As far as the many simulation works on EAS are concerned, a part from the quoted Ref. [1], only a limited fraction of them has considered the question of the time structure [13–23].

The interest in this topic has been renewed by recent experimental data concerning the detection of an anomalous delayed component [24]. In this framework it is therefore important to achieve a better and more detailed knowledge of this time structure. Furthermore, eventual fast simulation tools based of simple parametrisations constructed on this knowledge can be helpful not only for analysis, but also for design of new detectors, trigger evaluation, etcetera.

When a full shower simulation is considered, the structure of the time front depends to a large extent on the details of particle transport algorithms. Therefore, it can be useful to consider the outputs of very detailed codes, and compare it with the results of the codes optimized for the cosmic ray physics, which often contain simplifications in order to reduce the computer time. A valuable study of the time structure of Extensive Air Showers, for very high energies, based on the use of the CORSIKA code [25] has been presented in [3].

Here we present the study of the time structure of the e.m. secondary component generated by a photon or proton, as calculated mainly with the FLUKA96 code.

We have already used such code in [26], where we published the parametrisations of e.m. size resulting from photon and electron induced subshowers. Such code has already been successfully used in other cosmic ray applications [27,28].

We have explored primary energy from 100 GeV up to 100 TeV, injected at the top of the atmosphere. This energy range is of particular interest for gamma-astronomy purposes, mainly in the chance of possible differences in the time structure between gamma and proton initiated showers.

After describing the MC setup, we discuss the search for the best functional shape to fit the time distribution, and then results are discussed. Numerical results of characteristic parameters are given for different energies, secondary particles and detector altitudes.

2. The MC codes

Among the shower programs available in the High Energy Physics community, we have mainly considered FLUKA96 [29], although in some cases we have also used GEANT version 3.21 [30], using the interface to the FLUKA package (1992 version) for hadronic interactions. It must be stressed that GEANT-FLUKA and FLUKA96 are not the same thing, for different reasons: the e.m. simulation code is different [31], particle transport algorithms are different and, most of all, the FLUKA interface of GEANT contains only part (updated to 1993) of the hadronic interaction model of full FLUKA96.

In particular, the full FLUKA96 code employs transport algorithms with refined path length corrections [32] associated to multiple scattering, which are essential in problems involving low energy electrons and positrons. Furthermore, FLUKA96 is completely in double precision, thus allowing a much more accurate definition of a finely segmented geometry setup which extends itself up to many tens of kilometers. Another advantage coming from double precision is the timing accuracy even below 1 ns. An additional advantage of the full FLUKA96 package is the inclusion of very detailed models of nuclear excitation and low energy neutron transport. As we shall see in the following, this last topic has some importance for the argument of this paper. The two different codes

adopted in this work provide slightly different results, in particular for $\log_{10}t/ns \leq 0$, because of the insufficient precision of the GEANT transport algorithms. However, for $\log_{10}t/ns$ greater than that, the differences in the bulk of arrival time distributions are substantially within statistical fluctuations. For all these reasons, in the following sections we shall limit ourselves to the discussion of the results obtained with FLUKA96.

The atmosphere is defined by a stack of box volumes of rectangular basis and thickness increasing with the height above the sea level. Any volume corresponds to a depth of ~ 24 g/cm^2. In each box the density is uniform, and it is chosen in such a way that an approximation to the standard U.S. atmosphere is performed according to the Shibata fit [33]. The chosen depth granularity in our approximation is about one half of radiation length (37.66 g/cm^2) in air. We have limited the top of atmosphere at 1 g/cm^2, and the bottom is at 1025 g/cm^2. Particles have been injected at the altitude $H = 45.445$ km above the sea level. We have used the same elemental composition at all depths. The kinetic energy cut for secondary charged particles has been fixed to 1 MeV, while for secondary photons we have chosen 0.5 MeV in order to include the contribution from e^+e^- annihilation. Particles have been recorded at three different detector heights, corresponding respectively at sea level, and 1000 and 2000 m above sea level. These altitude values have been chosen in order to apply our work mainly to the case of the Gran Sasso laboratory site. For our investigation, we generated only vertical showers, at different log-spaced energies: 100, 177, 316, 562, 1000, 1778, 3128, 5623, 10000, 17780, 31620, 56230, 100000 GeV.

3. Analysis

We present results for different groups of secondary particles. We have considered separately photons, electrons (both e^+ and e^-) and other charged particles (muon, pions, etc.). The last group of secondary particles is relevant only in the case of primary hadrons. It must be noticed in fact that the adopted codes did not activate the hadro-production by photons.

As already done by other authors [4], we defined as relevant variable the time delay t with respect to a spherical front moving with light speed c, originating

from a fixed injection point of the atmosphere, i.e. we are giving the shower disk deviation from such a spherical front. The exact definition of our delay variable t is given by

$$t = t_{\text{arrival}} - \frac{\sqrt{H^2 + r^2}}{l} , \qquad (1)$$

where r is the distance from the shower core, and t_{arrival} is the arrival time of the considered secondary particle, as calculated by the code, and H is the injection point height in the atmosphere. The injection of the primary particle occurs by definition at zero time.

We have recorded the delay distribution in different radial bins from the impact point of the shower axis for each different group of secondary particles. On the basis of the features of the lateral distribution of secondary particles, we use a logarithmic spaced radial zones, for a total number of 9 regions:
- I: 0–4.64 m
- II: 4.64–10.00 m
- III: 10.00–21.54 m
- IV: 21.54–46.42 m
- V: 46.42–100.00 m
- VI: 100.00–215.44 m
- VII: 215.44–464.16 m
- VIII: 464.16–1000.00 m
- IX: 1000.00–2154.42 m

The contributions at a distance exceeding the limit of region 9 are negligible for the considered energies.

3.1. The arrival time probability distribution function

We paid a particular attention to the choice of a suitable function which can be used to fit the delay distribution in any of the considered radial regions. If there is no interest in time delays larger than tens of nanoseconds, usually a good choice in experimental analysis is the gamma function, as in Ref. [1] or [2],

$$\Gamma(t) = A \cdot t^{\beta} e^{-t \cdot \alpha} . \qquad (2)$$

However, the authors often note how the gamma function cannot account for the long tail of the experimental delay distribution [2].

Our simulations also exhibit such long tails, but we have found that the use of a log-normal function allows a fairly satisfactory reproduction of the simulated data (at least when no smearing effects due to

finite resolution of detector are included) in any of the aforementioned radial regions, up to a very long delay time ($\simeq 10 \ \mu s$),

$$f(t) = \frac{A}{t} \cdot e^{[-(\log t - B)^2 / C]} . \qquad (3)$$

The B and C parameters of such a distribution (essentially related to the mean delay and to its r.m.s) are also found to follow simple evolution as a function of shower energy and radial distance.

The preference for the log-normal behaviour could reflect some intrinsic feature of the underlying processes. According to Ref. [34], the log-normal distribution arises whenever we are in presence of a variable whose value takes a random proportion of that of the previous step in the stochastic process. However, we must stress that our choice of approximating function was an heuristic fact, aiming to the best approximation of the actual distribution. In fact, we did not adopt any mathematical model as input for the shower development, thus we merely state that the log-normal distribution provides a better numerical approximation than the gamma function to the phenomenological delay distribution. Therefore, also the concept of goodness of fit has to be somewhat relaxed in the present discussion with respect to a rigorous statistical context.

As an example, in Fig. 1 we show the time delay distribution for secondary gamma recorded at 2000 m a.s.l. in the radial region V, as produced by primary protons of energy 100 TeV, fitted up to 200 ns of delay, with log-normal and gamma functions.

The differences are self evident and can be noticed at different energies, radial regions, etc.

After this conclusion, we find it more convenient to reexpress all the results plotting $\log t$ instead of t and then fitting to a Gaussian, as shown in the upper part of Fig. 2, which refers to the same case of Fig. 1. The distribution for secondary e^+e^- has practically a log-normal shape. It is also interesting to look at the distribution, for the same energy, radial bin, etc., when secondary muons and charged hadrons are selected. This is shown in the bottom part of Fig. 2.

The resulting distribution, for this primary energy and distance from the core, is even more asymmetric than that of electrons or photons. The consequence is that neither the pure gamma or the pure log-normal distribution succeed in fitting the delay distribution up to large t values. At smaller distances from the core,
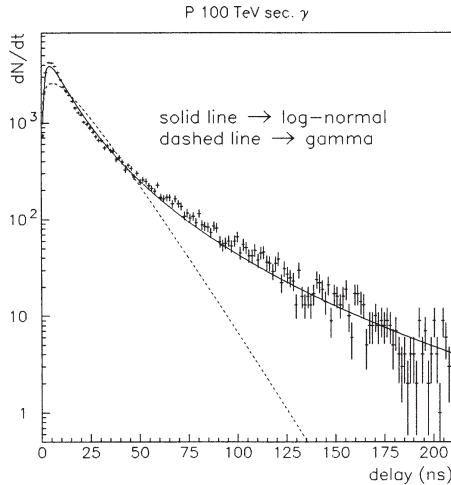
P 100 TeV sec. γ

Fig. 1. Log-normal and Gamma fit to the delay distribution of secondary γ's and from primary 100 TeV protons, as detected at 2000 m a.s.l. in the V radial region (stand-alone FLUKA96 simulation).
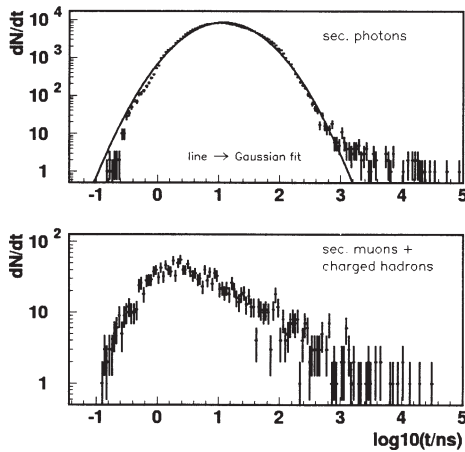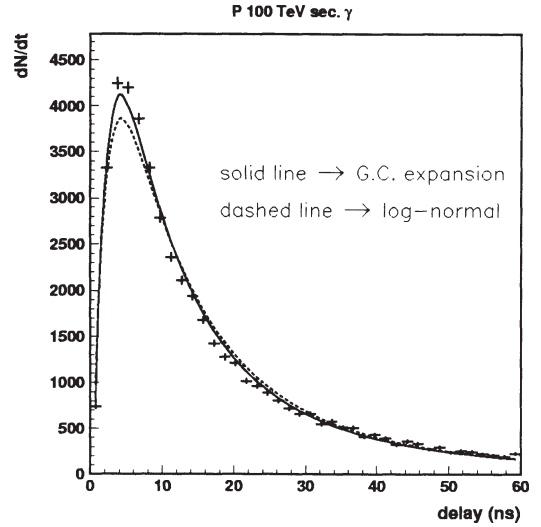

Fig. 2. Above: Gaussian fit to the $\log_{10} t$ distribution of secondary γ's and from primary 100 TeV protons, as detected at 2000 m a.s.l. in the V radial region (stand-alone FLUKA96 simulation). Below: $\log_{10} t$ distribution of secondary muons and charged hadrons, for the same primary energy and distance from the shower core.

also for muons and charged hadrons, the log-normal approximation works better. However, in the following, we shall limit ourselves to the discussion of the results for $e^+ e^-$ and γ's, since their density largely dominates that of muons, or residual charged hadrons. We recognize that the case of muons and other charged particle would deserve a dedicated study, also in view of the fact that it has been recently advocated the use of the arrival time of muons for measurements re-

lated to the mass composition of primary cosmic rays, using the so-called "Time Track Complementarity" (TTC) [35]. At present we are not able to perform with our tools a detailed study of this method, since our Monte Carlo code does not allow, in this version, the treatment of nuclear projectiles and the primary energies required for this purpose.

In any case, it already appears that also the log-normal fit is not sufficient to weight carefully the whole t range. Such a fit usually takes good care of the bulk of the events, but the extreme tails of the $\log t$ distributions exhibit deviations from a perfect Gaussian behaviour. As a matter of fact, the left tail is very important, since it corresponds to the early front of the shower that affects the experimental trigger time. The right tail refers to the very delayed component of EAS. In order to look for a more precise description of the simulation results, we characterise the $\log_{10} t$ distribution and its deviations from a pure log-normal one by means of a set of parameters. We find convenient the use of central moments (i.e., the moments calculated around the mean). Starting from the values of a finite set of these moments, the distribution can be reproduced (and directly sampled in Monte Carlo) with a sufficient degree of approximation, as demonstrated in Ref. [36]. We consider a variable ξ defined by $\xi = \log_{10}(t) - \mu_1/\sigma$, where μ_1 and σ are the average and the r.m.s. of the $\log_{10}(t)$ distribution. If the $f(\xi)$ distribution function (p.d.f. in the following) can be approximated by a standard normal $g(\xi)$, then $f(\xi)$ can be expanded in series of the derivatives of the standard normal function,

$$f(\xi) = g(\xi) \left\{ 1 + \frac{\mu_3}{6\sigma^3} H_3 + \frac{1}{24\sigma^4}(\mu_4 - 3) H_4 + \frac{\mu_3^2}{72\sigma^6} H_6 + \cdots \right\}, \qquad (4)$$

where H_n are the Hermite polynomials of order n and μ_n are the central moments of $f(\xi)$,

$$\mu_n = \sum_{i=1}^{N} \frac{(\log_{10}(t_i) - \mu_1)^n}{N}. \qquad (5)$$

This is also known as the Graham–Charlier expansion (GC in the following). We have chosen to give the first four moments of $\log_{10}(t)$ distributions. This set seems sufficient to express the features of the delay

distributions in most cases, but there are some limitations, as discussed in the literature, which would demand for higher order moments. For instance, when μ_4 increases above a certain limit, moments of an order greater than $n = 4$ must be considered in the expansion, otherwise the distribution becomes neither unimodal neither positive defined in the whole range.

However, we must stress how the moments of high order are subject to statistical fluctuations in case of a small number of entries in a distribution. In that case the errors induced by such fluctuations might be even larger than that due to the omission of such moments.

To show how the G.C. expansion works, in Fig. 3 we show the comparison between the pure log-normal and the GC expansion fits to the short delay region of the same distribution of Fig. 1 (please note the linear scale!). Such an improvement can be seen also at large delays.

In summary, a better χ^2 is obtained but usually the first two moments resulting from the fit, common to the two functions, are the same within the fit errors for the two case. We stress that, for most of the cases, these first two moments (i.e., the log-normal approximation) are sufficient to describe the time delay distribution from the experimental point of view (i.e., $\log(t/ns) > 0$), with the noticeable exception of long tails at large radial bins for proton showers, as will be discussed in Section 5.

An important outcome of the series expansion in terms of moments is that it is possible to derive an expression which allows to have a direct Monte Carlo sample of the the desired p.d.f. with good accuracy starting from a random number normally distributed ξ without any rejection. This is described and demonstrated in [36]. The relation between variable x to be generated with average μ, standard deviation σ and central moments μ_n, and the normal distributed number ξ is given by

$$
\begin{aligned}
x = \mu + \sigma \Bigg[&\xi + \frac{\mu_3}{6\sigma^3}(\xi^2 - 1) \\
&+ \frac{\mu_4 - 3\mu_2^2}{24\sigma^4}(\xi^3 - 3\xi) \\
&- \frac{\mu_3^2}{36\sigma^6}(2\xi^3 - 5\xi) \Bigg],
\end{aligned}
\tag{6}
$$

with the μ_n giving the nth central moments of the x distribution function. Of course $\mu_2 = \sigma^2$.

Fig. 3. Log-normal and GC fits to the small delay region of the distribution of secondary γ's and from primary 100 TeV protons, as detected at 2000 m a.s.l. in the V radial region (stand-alone FLUKA96 simulation.
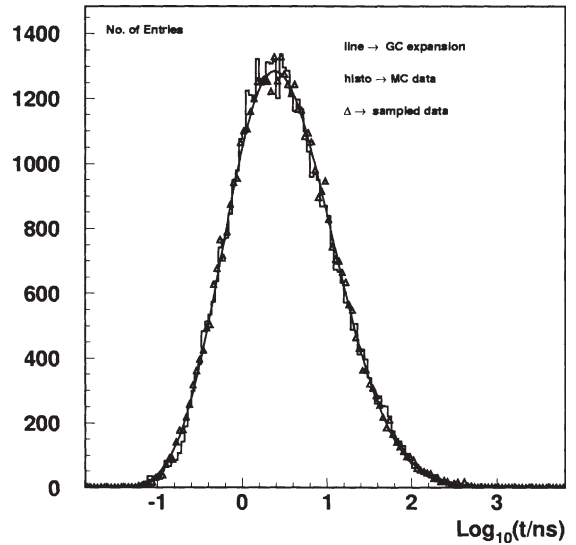
Fig. 4. Comparison between the M.C. data the momentum expansion and the sampling described in [36].

An example of the functionality of this sampling method is shown in Fig. 4 where the M.C. output, the momentum expansion and the sampled data from this expansion are superimposed.

Further differences, such as those discussed in Section 5, can be considered as an estimate of the systematic error related to the choice of different MC algorithms and interaction models.

4. Results

In this section we present the M.C. results giving information about the four moments that appear in the expansion of Eq. (6), for different sets of primary particle, secondary produced and distance from the shower core (radial bin). For practical convenience, instead of μ_2, μ_3, μ_4, in the following we shall use r.m.s ($\sqrt{\mu_2}$), skewness ($\mu_3/\mu_2^{3/2}$) and kurtosis ($\mu_4/\mu_2^2 - 3$) in place of μ_3 and μ_4. For each set of the three quoted parameters, we obtained these quantities in two ways: by direct computation of the moments from the logarithm of the arrival times, and by fitting the $\log(t)$ distribution with the GC expansion with the moments used as fit parameters. A quantitative comparison of this two set of moments is made using the computed one as fixed parameters of the GC function and fitting the $\log(t)$ histogram with only the normalisation as a free parameter. In most cases, the two sets of resulting moments are in good agreement, within the errors, and also the χ^2 values from the two fits are similar. Important exceptions are those relative to the regions where we had low statistics. There, the moments obtained from the general fit generally give a worse approximation of the data than those directly computed.

We will show how the behaviour of the parameters is rather smooth, so that all intermediate cases in radius and detection height can be easily obtained by interpolation. We shall express the results in two ways: we will consider the moments of the average time distribution of single secondary particles (i.e., the distributions obtained summing the arrival times for each particles and for all the primary showers), but we shall also give quantitative information on the statistical fluctuations of these moments from event to event. Unfortunately, our simulation runs at the highest energies have only a small number of events, so that while the single particle distribution is always measured with high accuracy, the fluctuations on an event by event basis are studied with less precision.

4.1. The p.d.f. moments

The obtained moments [1] for the distributions recorded at the observation level of 2000 m a.s.l. are given in the tables reported in the appendix. As previously stated, we limit ourselves to the results for secondary e^+e^- and γ, which dominate the shower size. We refer mainly to the level of 2000 m a.s.l. since, in applications like gamma-astronomy, it is the most favourable among the three a priori foreseen observation levels, although higher altitudes would be even more appealing for this purpose. The tables of parameters at the other lower observation levels can be obtained from the authors.

In this section we present a subsample of these results in a graphical way in order to discuss the essential features. We plot the moment values without the corresponding error as derived from the fit. This is because those errors are dominated by the generated statistics and are smaller than the actual shower to shower fluctuations, which instead are specifically reported in this paper. There is also another important comment about these results. Since the moments have been extracted from a fit, there exists some degree of correlation among them. This makes even less significant the error on a single parameter. We cannot report here the covariance matrix for all the relevant cases, and the irregularities visible in these figures are not simply due to statistical fluctuations. Correlations are such that the evolution of the resulting distribution is much smoother than that of single parameters.

In Fig. 5 the moment values are shown versus the logarithm of the primary energy for three radial bins, for the case of showers induced by γ primaries and in Fig. 6 are plotted the same quantities for proton induced showers.

The most striking feature is that the average value of $\log(t)$ is almost independent from primary energy (at least in the range considered by our simulation), the kind of primary or secondary particle, and changes only with the radial bin.

If we adopt the log-Gaussian approximation, we remind that, for this distribution, the correspondence between $\langle t \rangle$, σ_t and $\langle \log_{10}(t) \rangle$, μ_2 is given by

---

[1] For the sake of simplicity, we shall use in the following the term moment, although r.m.s, skewness and kurtosis are not the true moments.

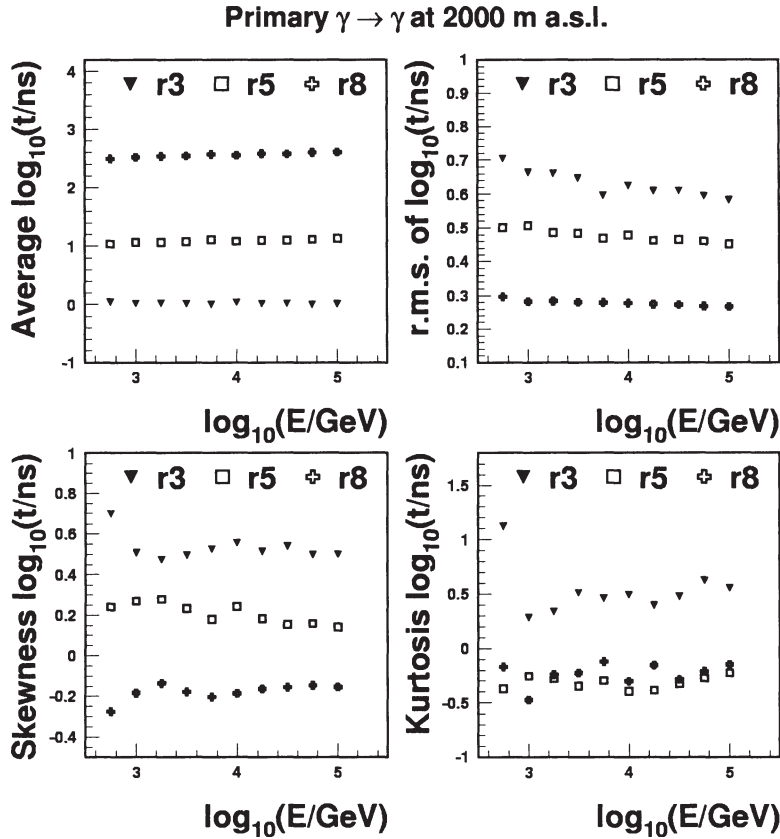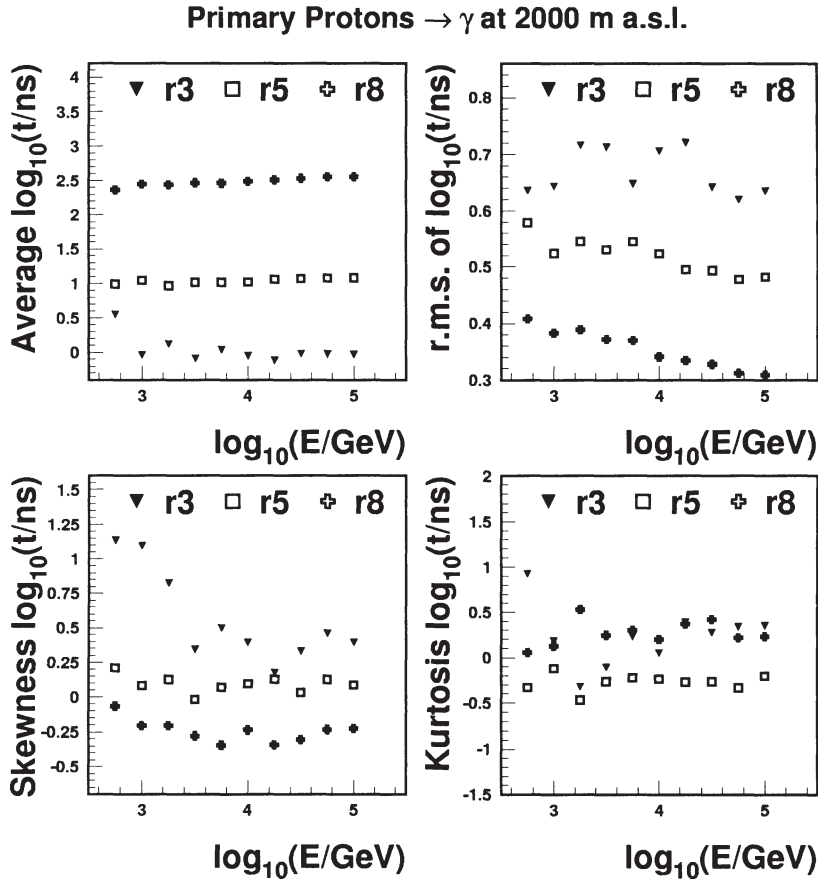**Primary γ → γ at 2000 m a.s.l.**

Fig. 5. First central momenta of the arrival time p.d.f. versus $\log(E)$ for secondary γ from γ primary in 3 different radial bins. Here r3, r5, and r8 stand for radial bin III, V and VIII.

$$\log_{10}\langle t\rangle = \langle \log_{10}(t)\rangle + \frac{\mu_2}{2}\log_e(10) , \qquad (7)$$

$$\sigma_t = \langle t\rangle \sqrt{(10^{\mu_2 \log_e(10)} - 1)} . \qquad (8)$$

The increase in the average delay (which we remind is measured with respect to a light ray) as a function of distance from the shower core reflects the fact that moving to the outer regions of the shower, the average energy of secondary particles decreases, and therefore the deviations from a straight line trajectory become more important.

The values of $\sqrt{\mu_2}$ are slightly different according to the different primary or secondary species, but is substantially constant with respect to the primary energy for γ induced shower and shows a weak dependence from this parameter for proton primary. We also notice an apparent reduction of the variance (i.e., a shrinkage of the distribution) as function of the radial distance from the core. One should not be induced in error, since we plot the variance of $\log t$: it can be verified that transforming back to the t variable, the effective width of the delay distribution (directly related to the time thickness of the shower disk) increases as a function of distance. Let us take a numerical example; for a primary gamma of 10 TeV, we have a r.m.s. around 0.6 in the third radial bin, when the average is 0.004. It means that the 68% fraction in $\log t$ is in the range 0.18–6.0 ns. Instead, in the eighth radial bin, the r.m.s. drops 0.28, while the average increases to 2.6. Therefore, the 68% fraction in $\log t$ is now in the range 118–1350 ns.

The higher moments are very different for the two primaries: roughly speaking the proton induced showers have higher third and fourth moments, that is, the $\log(t)$ p.d.f. has a less log-normal shape. In order to

Fig. 6. First central momenta of the arrival time p.d.f. versus $\log(E)$ for secondary γ from proton primary in 3 different radial bins. Here r3, r5, and r8 stand for radial bin III, V and VIII.

understand that, but also to give a clearer idea of the evolution of time delay distributions, we show in Fig. 7 the $\log t$ distributions at 10 TeV for γ and proton showers in few different radial bins. We can clearly see that while there is a nearly log-Gaussian bulk almost identical in the two cases, an additional tail at high delays appears for proton showers, particularly visible at large distance from the shower core. Our fit is unable to follow completely this tail, which presents itself as a distinct family of particles. Indeed the population of these highly delayed particles is only a very small fraction of the total number of arriving e.m. particles. We postpone the specific discussion on this phenomenology in Section 5. Coming back to the general features of the delay distribution, we stress that the extracted moments describe the average arrival time distribu-

tion functions. Obviously, remarkable fluctuations can be detected in a event-by-event analysis of the generated data. For example, in Fig. 8 we superimpose the electron arrival time distribution for 4 different showers induced by a 100 TeV γ primary. The differences in shape and normalisation for the different showers are evident. This effect is amplified in the showers induced by proton primaries. This is highly correlated to the large fluctuations in the height of the first inelastic interaction. In Fig. 9 are presented the momenta fluctuation for γ primaries, to be compared with much bigger fluctuation presented in Fig. 10, corresponding to the proton primaries. As expected, all the fluctuations shows a decreasing behaviour with the energy.

Table 1
Percentage of delayed particle and relative abundance of neutrons, photons and electrons for different radial bins, in EAS induced by a 100 TeV proton primary

Rad. bin	Time thr.	$\dfrac{N_{\text{delayed}}}{N_{\text{total}}} \times 10^{-4}$	$\dfrac{N_\gamma}{N_{\text{delayed}}}$	$\dfrac{N_{neutrons}}{N_{\text{delayed}}}$	$\dfrac{N_{e^+e^-}}{N_{\text{delayed}}}$
II	$\geq 10^2$ ns	9.3	89.5 (%)	3.5(%)	7.0(%)
V	$\geq 10^3$ ns	5.4	30.0 (%)	59.0 (%)	4.0(%)
VIII	$\geq 10^4$ ns	196.8	6.5 (%)	93.0 (%)	0.5(%)
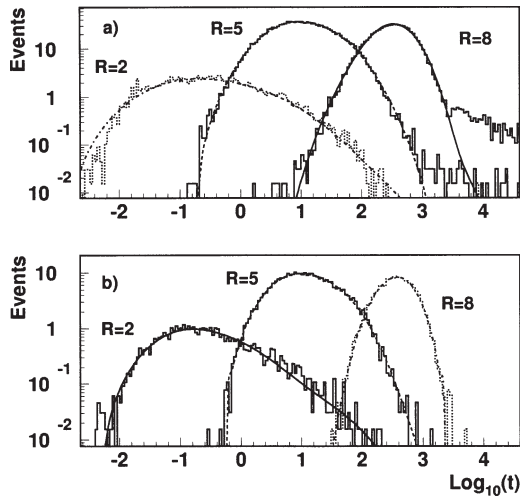
Fig. 7. $\log_{10} t$ distributions at 10 TeV for proton (above) and γ (below) showers in few different radial bins. Here r2, r5, and r8 stand for radial bin III, V and VIII.
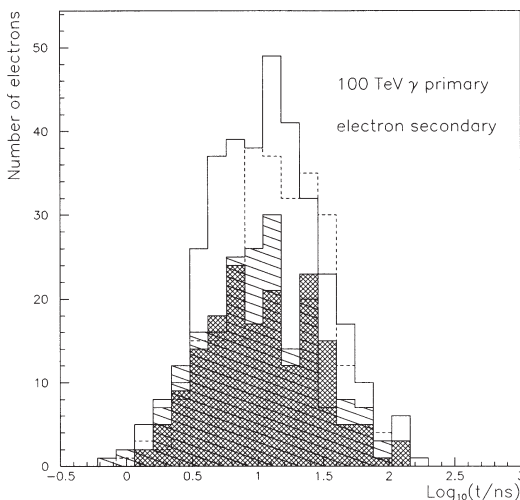
Fig. 8. Electrons arrival time distributions for single showers from gamma 100 TeV primary.

5. Discussion of the origin of delayed particles

The time structure of e^+e^- and γ secondaries from hadronic and pure e.m. showers shown in Fig. 7 is rather similar, as far as the nearly log-Gaussian bulk is concerned. The main difference consists in the appearance, in the hadronic showers, of a slow e.m. component which becomes more and more visible at large distance from the shower core. Such a component seems to constitute a different family, really well separated from the major population. It can extend itself up to tens of microseconds. We have investigated in some detail the simulation steps, in order to understand the physical origin of such a delayed component. We have learned, of course, that the bulk of our time delay distribution come from the relativistic part of the shower, namely from the e.m. showers coming from π_0 decay. Instead, the delayed family in hadronic showers comes from the de-excitation of air nuclei after the interactions with neutron of energy below few tens of MeV. These neutrons are quite slow, and for this reason separate easily from the relativistic component. Of course, this secondary electro-magnetic component is a small fraction of a much larger population of neutrons which dominates the shower disc at large distances. Table 1 shows the percentage fraction of delayed particles, neutrons, γ and electrons, above a radial dependent time threshold, for 100 TeV proton primary at 2000 m a.s.l. The time threshold for a given radial bin has been chosen in such a way to approximately define the transition region between the log-normal bulk and the additional tail.

The treatment of nuclear effects, and in particular of de-excitation processes, is one of the most interesting feature offered by the FLUKA code. The description of the modelization of these processes is given in Refs. [37,38]. We have to notice that also in the

FLUKA interface of GEANT 3.21 a nuclear evaporation model is present, but it much more simplified and approximated with respect to that of the quoted references. We are aware that this new evaporation model is now also interfaced to CORSIKA [25], version 5.60, when the DPMJET interaction model [39] is chosen. However, such a package in the frame of CORSIKA is not yet available for public distribution.

Here we try to summarize the possible different low-energy reactions which can contribute to the process under investigation.

(a) Capture reactions (n, γ): very probably these are not the relevant phenomena in our case, since these would give photons with much larger delays than those considered in our distributions. However, in general they have a small cross section. This reaction can be relevant for Ar (630 mbarn) through the process $^{40}Ar(n, \gamma)^{41}Ar$. On this respect we have to make the following remark. The present simulation has been performed in the case of a dry atmosphere, but in case of a relevant presence of humidity in air or near the soil (in presence of snow for instance), the build-up of capture reactions can be relevant due to the thermalization of neutrons on H nuclei.

(b) Reactions (n, n'), where the neutron is scattered leaving the nucleus in an excited state. The residual nucleus will decay to the ground state emitting a cascade of photons between the different levels. This phenomenon is one of the most important sources of delayed photons, since an energy just above the first excited level is enough. For N, the first three excited levels are at 2.319, 3.948, 4.915 MeV. For Ar they are at 1.461, 2.121, 2.524 MeV, while for O they are at 6.049, 6.130, 6.919 MeV (therefore, this reaction is less relevant in the O case). The excitation of higher levels is usually negligible. The lifetime of these excited levels is quite short (ns scale or less), so that these photons are promptly emitted. Furthermore, the model makes use of an isotropic angular distribution. This is not very different from reality.

(c) There are also reactions with production of other particles together with additional γ's. We can quote, in order of increasing energy threshold:

- (n, p); among these, an important exception is the celebrated $^{14}N(n, p)^{14}C$, which does not produce γ's;
- $(n, 2n)$; this is practically closed for O nuclei below about 20 MeV, but is open for the other nuclei of

air even at lower energies;
- (n, α);
- (n, d);
- (n, t);
- (n, kp), with k produced protons;
- $(n, k\alpha)$, with k produced α's.

For each of these processes, the cross section rises quite fast above the threshold.

The reason why we notice the delayed family at large distance is that the low energy neutrons can be found more easily in the periphery of the shower, where energy is degraded. Furthermore, this nonrelativistic component is obviously much more smeared in space than the relativistic one. Of course, the delayed neutron component can give much larger signals in a given detector (for instance in a scintillator array) with respect to the associated secondary e.m. component. However, we would like to stress that in case of nuclear projectiles (a case outside the scope of the present simulations) we shall have also excitation of the nuclear fragments coming from the projectile. Unlike the case of the excitation of the target nuclei, the photons (and other particles) following the de-excitations of the fast moving fragments will be Lorentz-boosted in the laboratory frame, in order to contribute in a more efficient way to the energy deposition. In particular, we advance the hypothesis that they can give rise to subshowers having some delay with respect to the first particles in the EAS disc. For instance, we suggest that this could be the basis for an explanation of the observation of a delayed component [24] in VHE Extensive Air Showers, as observed in the COVER-PLASTEX detector in the GREX array [2].

We wish to point out that the inclusion of these processes in simulation codes for high energy cosmic ray physics has not yet become a common practice. Therefore, these phenomena might have escaped from other simulation studies, while the existence of such delayed particles might have some experimental relevance.

6. Comparison with experiments

We compare our results with the EAS-TOP [4] array experimental data. In Fig. 11 we plot the average secondary delay from the first particle, with respect to the radial bin. This values refer to the photons pro-
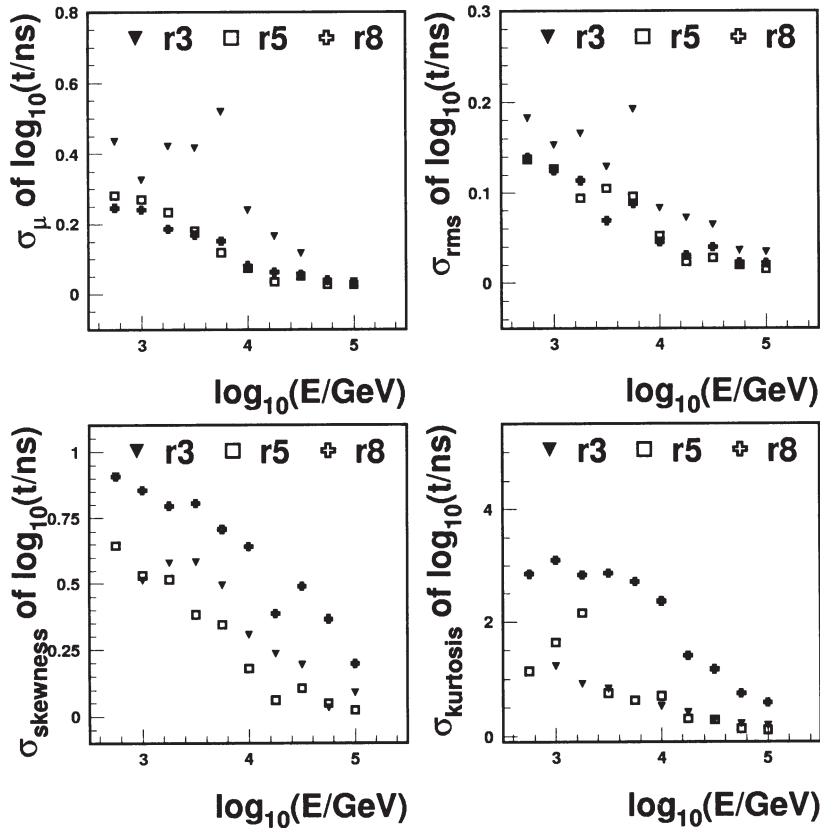
Primary $\gamma \rightarrow \gamma$ at 2000 m a.s.l.
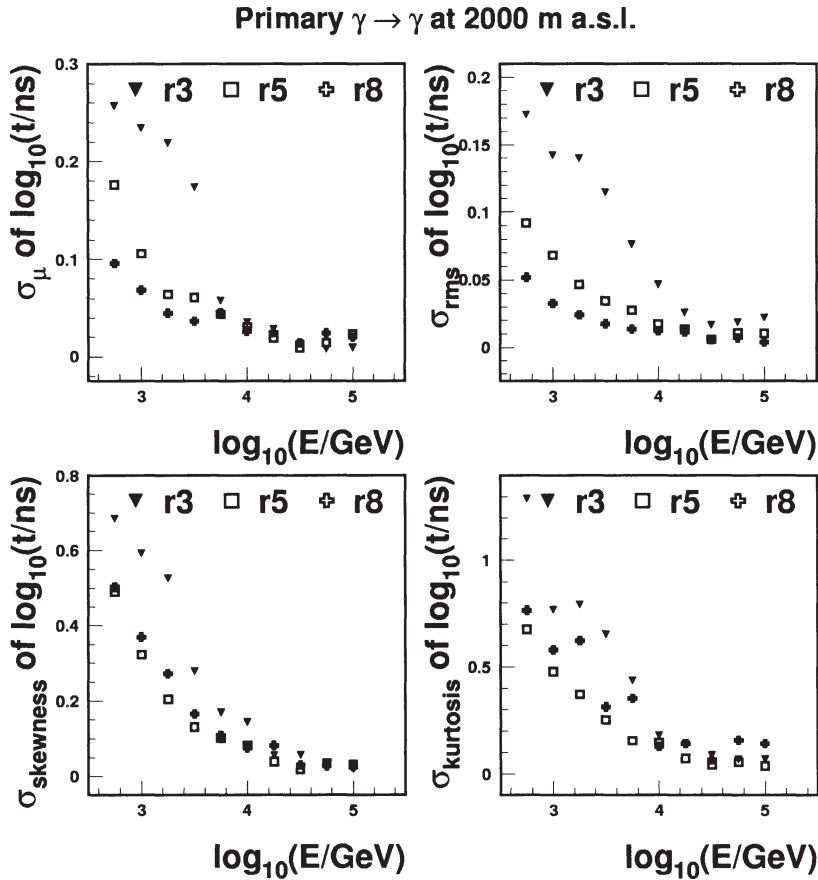
Fig. 9. Fluctuations of first central momenta of the arrival time p.d.f. versus $\log(E)$ for secondary γ from proton primaries. Here r3, r5, and r8 stand for radial bin III, V and VIII.

duced by a 100 TeV, proton initiated EAS as detected at 2000 m a.s.l. The EAS-TOP signal is dominated by the secondary electrons, but we remark that, at least in this range of parameters, the differences with respect to the time distribution of secondary electrons appear to be very small. On the other hand, the number of photons is much larger [26], and this allows a reduced statistical uncertainty. The average value we obtain seems to reproduce the EAS-TOP experimental data. These are divided in 2 samples, corresponding to the cases in which they had at least 1 or 4 particles in each of the triggered sub-detectors. The event class corresponding to at least 1 particle in the detector should correspond to a primary energy close to the trigger threshold of EAS–TOP ($\simeq 100$ TeV, mostly from proton primary). At distances from the core lower than

100 m, the two classes are not distinguishable. In the same figure we also show that our results are systematically higher than those of Ref. [1]. There the calculation was done only for *gamma* primaries, but our results, in the same range of distance from the shower core, do not exhibit substantial differences between the two species of primaries [2]. Also the delay distribution width (that is the shower disk thickness), is well reproduced by our simulation: in Fig. 11 is reported the width of the delay distribution as measured at 70% of the height of the peak, for different radial bins. The

---

[2] We must note, however, that the numbers from Ref. [1] were obtained using a threshold at 5 MeV. In a more recent paper [40], Di Sciascio et al. describe new calculations performed with 1 MeV threshold. In that case, their results exhibit a much better consistency with our calculations.

Primary Protons → γ at 2000 m a.s.l.

Fig. 10. Fluctuations of first central momenta of the arrival time p.d.f. versus log(E) for secondary γ from proton primaries. Here r3, r5, and r8 stand for radial bin III, V and VIII.

agreement between Monte Carlo and the EAS-TOP data is very good. In spite of the goodness of the simulation results we want to stress the effect of a finite detector resolution on the simulated arrival time of the secondaries. In particular, in the first radial bins (near the axis of the shower), the arrival time distribution are peaked at time values which can be lower than the typical experimental time resolution. Thus the result of the folding of the simulated p.d.f. with the experimental error distribution drastically modifies the distribution in these radial bins, producing a flattening at arrival times close to the time resolution value.

This effect is shown in Fig. 12 where we plotted a log-normal function with $\langle \log_{10}(t/ns) \rangle = -0.54$ and $\sigma_{\log_{10}(t/ns)} = 0.75$ (similar to the delay distribution expected at 2000 m.a.s.l for secondary photons from

primary gamma, in the 2nd radial bin), superimposed to the same distribution folded with a Gaussian error function with $\sigma_{exp} = 1$ ns. The effect of the experimental resolution is clearly seen on the bulk of the events, even if the average value of the arrival time is bigger then the resolution value.

We remark also that usually the experimental results are expressed as particle delay distribution as measured since the arrival of the experimental trigger. This is different from the delay time from the light cone that we used in M.C. These two distributions are almost equal if the shower is so populated that the first triggering particle has a minimum delay from the light cone, but can be quite different for low statistic showers, where the triggering particle may arrive after a sizeable delay from the light cone. In this case the
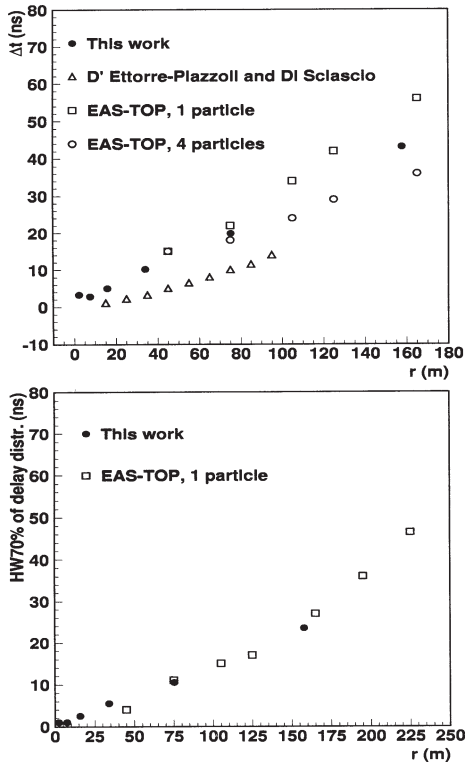
Fig. 11. Average particle delay from the first arrived particle and width of the delay distribution at 70% of the peak vs the shower axis distance for 100 TeV primary protons (see text for details).
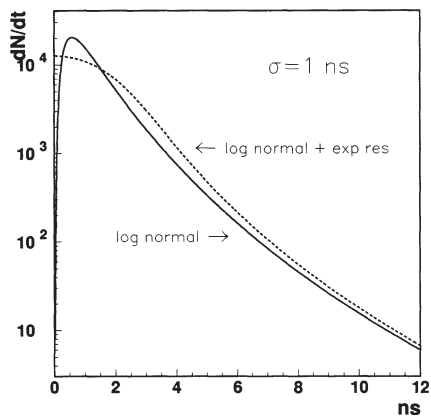
Fig. 12. Effect of the folding of a Gaussian experimental resolution ($\sigma = 1$ ns) with a log-normal distribution, similar to the delay distribution expected at 2000 m a.s.l for secondary photons from primary gamma, in the 2nd radial bin.

M.C. distribution are biased toward the longer delays with respect to the experimental results by an amount of time given by the average delay of the first particle.

7. Conclusion

We have simulated the time delay of vertical Extensive Air Showers by means of the FLUKA Monte Carlo code. We have shown how the logarithm of the time delay distribution of a shower front can be easily expressed as a Gaussian expansion in terms of a few parameters. Such parameters exhibit a smooth behaviour as a function of energy, thus allowing the extrapolation to higher energies of the presented Monte Carlo simulation results.

The proposed expansion allows the construction of fast algorithms useful in detector design and data interpretation, when the running of a complete detailed simulation would result in unnecessary heavy job. Differences between protons and gamma initiated showers are observed. In particular, hadronic showers exhibit a delayed component at large distance from the shower axis. These differences have been interpreted as due to effects coming from nonrelativistic particles in the shower. In particular, we found that the deexcitation of air nuclei following the interaction with low energy neutrons are the essential contributions to the highly delayed e.m. component in hadronic showers. We remark how this can be obtained at simulation level, only with very specialized and detailed codes, not commonly used so far in cosmic ray physics. In particular situations, these results can be used as an interpretation basis for the understanding of apparently anomalous delays.

Acknowledgements

Appendix A. Tables of moments and of their fluctuations

Table A.1

Central momenta for the distribution function of $\log(t/ns)$ for secondary γ produced at 2000 m a.s.l. by a γ primary, as obtained from the FLUKA stand-alone simulation. Primary γ, Sec. γ, h_{det} = 2000 m a.s.l.

Rad. bin	Average	Sigma	Skewness	Kurtosis
E_0 = 562. GeV				
1	$-.77\pm$ .45	$1.03\pm$ .28	$.3\pm$ .7	$3.2\pm$ 1.1
2	$-.35\pm$ .30	$.83\pm$ .19	$.5\pm$ .6	$3.0\pm$ .7
3	$.05\pm$ .26	$.71\pm$ .17	$.7\pm$ .7	$4.1\pm$ 1.3
4	$.51\pm$ .25	$.61\pm$ .15	$.3\pm$ .6	$3.1\pm$ .9
5	$1.04\pm$ .18	$.50\pm$ .09	$.2\pm$ .5	$2.6\pm$ .7
6	$1.54\pm$ .12	$.44\pm$ .07	$.0\pm$ .4	$2.5\pm$ .6
7	$2.04\pm$ .10	$.36\pm$ .05	$-.2\pm$ .4	$2.6\pm$ .6
8	$2.49\pm$ .10	$.30\pm$ .05	$-.3\pm$ .5	$2.8\pm$ .8
9	$2.91\pm$ .11	$.24\pm$ .07	$-.2\pm$ .6	$3.0\pm$ .7
E_0 = 1000. GeV				
1	$-1.12\pm$ .41	$1.01\pm$ .23	$.5\pm$ .4	$3.1\pm$ 1.0
2	$-.37\pm$ .30	$.79\pm$ .24	$.3\pm$ .5	$3.0\pm$ 1.0
3	$.02\pm$ .23	$.66\pm$ .14	$.5\pm$ .6	$3.3\pm$ .8
4	$.53\pm$ .19	$.58\pm$ .09	$.4\pm$ .4	$3.1\pm$ .7
5	$1.06\pm$ .11	$.51\pm$ .07	$.3\pm$ .3	$2.7\pm$ .5
6	$1.56\pm$ .08	$.42\pm$ .05	$.0\pm$ .2	$2.5\pm$ .4
7	$2.06\pm$ .07	$.35\pm$ .03	$-.2\pm$ .3	$2.6\pm$ .4
8	$2.51\pm$ .07	$.28\pm$ .03	$-.2\pm$ .4	$2.5\pm$ .6
9	$2.92\pm$ .08	$.23\pm$ .05	$.0\pm$ .5	$2.6\pm$ .7
E_0 = 1778. GeV				
1	$-1.16\pm$ .32	$.99\pm$ .24	$.2\pm$ .9	$2.9\pm$ 1.6
2	$-.47\pm$ .33	$.79\pm$ .17	$.6\pm$ .5	$4.3\pm$ 1.1
3	$.02\pm$ .22	$.66\pm$ .14	$.5\pm$ .5	$3.3\pm$ .8
4	$.55\pm$ .12	$.57\pm$ .08	$.3\pm$ .3	$3.1\pm$ .6
5	$1.06\pm$ .06	$.49\pm$ .05	$.3\pm$ .2	$2.7\pm$ .4
6	$1.58\pm$ .05	$.42\pm$ .03	$.0\pm$ .2	$2.5\pm$ .3
7	$2.07\pm$ .05	$.34\pm$ .02	$-.2\pm$ .2	$2.5\pm$ .3
8	$2.53\pm$ .05	$.28\pm$ .02	$-.1\pm$ .3	$2.8\pm$ .6
9	$2.94\pm$ .06	$.23\pm$ .05	$.0\pm$ .5	$2.9\pm$ .7
E_0 = 3162. GeV				
1	$-1.04\pm$ .37	$.94\pm$ .20	$.8\pm$ .6	$4.5\pm$ .9
2	$-.53\pm$ .25	$.73\pm$ .15	$.6\pm$ .4	$4.1\pm$ .9
3	$.02\pm$ .17	$.65\pm$ .11	$.5\pm$ .3	$3.5\pm$ .7
4	$.55\pm$ .08	$.56\pm$ .05	$.4\pm$ .2	$2.9\pm$ .4
5	$1.07\pm$ .06	$.48\pm$ .03	$.2\pm$ .1	$2.7\pm$ .3
6	$1.59\pm$ .04	$.41\pm$ .02	$.0\pm$ .1	$2.4\pm$ .2
7	$2.08\pm$ .04	$.34\pm$ .02	$-.2\pm$ .1	$2.6\pm$ .2
8	$2.54\pm$ .04	$.28\pm$ .02	$-.2\pm$ .2	$2.8\pm$ .3
9	$2.96\pm$ .05	$.23\pm$ .03	$-.1\pm$ .3	$3.0\pm$ .5

Table A.1 — continued

Rad. bin	Average	Sigma	Skewness	Kurtosis
E_0 = 5623. GeV				
1	$-1.44\pm$ .32	$.95\pm$ .17	$.1\pm$ .5	$4.2\pm$ .7
2	$-.54\pm$ .13	$.66\pm$ .09	$.7\pm$ .4	$4.0\pm$ .8
3	$.00\pm$ .06	$.60\pm$ .08	$.5\pm$ .2	$3.5\pm$ .4
4	$.57\pm$ .04	$.53\pm$ .04	$.4\pm$ .1	$3.1\pm$ .2
5	$1.10\pm$ .04	$.47\pm$ .03	$.2\pm$ .1	$2.7\pm$ .2
6	$1.62\pm$ .05	$.40\pm$ .02	$-.05\pm$ .08	$2.6\pm$ .1
7	$2.11\pm$ .05	$.33\pm$ .01	$-.20\pm$ .08	$2.7\pm$ .2
8	$2.56\pm$ .05	$.28\pm$ .01	$-.2\pm$ .1	$2.9\pm$ .4
9	$2.97\pm$ .06	$.23\pm$ .01	$.0\pm$ .2	$2.6\pm$ .3
E_0 = 10000. GeV				
1	$-1.02\pm$ .28	$.98\pm$ .11	$.7\pm$ .3	$5.0\pm$ .6
2	$-.56\pm$ .12	$.73\pm$ .08	$.6\pm$ .3	$3.7\pm$ 1.1
3	$.03\pm$ .04	$.62\pm$ .05	$.6\pm$ .1	$3.5\pm$ .2
4	$.55\pm$ .03	$.55\pm$ .04	$.38\pm$ .06	$3.1\pm$ .2
5	$1.08\pm$ .03	$.48\pm$ .02	$.24\pm$ .08	$2.6\pm$ .1
6	$1.59\pm$ .03	$.41\pm$ .01	$.01\pm$ .05	$2.46\pm$ .09
7	$2.09\pm$ .02	$.34\pm$ .01	$-.14\pm$ .07	$2.6\pm$ .1
8	$2.55\pm$ .03	$.28\pm$ .01	$-.19\pm$ .07	$2.7\pm$ .1
9	$2.96\pm$ .03	$.23\pm$ .01	$.0\pm$ .2	$2.9\pm$ .4
E_0 = 17780. GeV				
1	$-1.20\pm$ .15	$.85\pm$ .06	$.7\pm$ .2	$3.4\pm$ .3
2	$-.53\pm$ .05	$.70\pm$ .04	$.6\pm$ .1	$3.7\pm$ .3
3	$.02\pm$ .03	$.61\pm$ .03	$.51\pm$ .06	$3.4\pm$ .1
4	$.55\pm$ .02	$.53\pm$ .02	$.35\pm$ .04	$3.0\pm$ .1
5	$1.10\pm$ .02	$.46\pm$ .01	$.18\pm$ .04	$2.62\pm$ .07
6	$1.62\pm$ .03	$.40\pm$ .01	$-.01\pm$ .02	$2.58\pm$ .06
7	$2.12\pm$ .03	$.33\pm$ .01	$-.18\pm$ .04	$2.6\pm$ .1
8	$2.58\pm$ .02	$.27\pm$ .01	$-.16\pm$ .08	$2.8\pm$ .1
9	$3.00\pm$ .03	$.23\pm$ .01	$.0\pm$ .1	$3.0\pm$ .2
E_0 = 31620. GeV				
1	$-1.28\pm$ .16	$.89\pm$ .03	$.5\pm$ .1	$3.6\pm$ .2
2	$-.52\pm$ .01	$.68\pm$ .02	$.70\pm$ .09	$3.7\pm$ .2
3	$.02\pm$ .01	$.61\pm$ .02	$.54\pm$ .06	$3.48\pm$ .09
4	$.56\pm$ .01	$.54\pm$ .02	$.39\pm$ .05	$2.98\pm$ .05
5	$1.10\pm$ .01	$.46\pm$ .01	$.15\pm$ .02	$2.67\pm$ .04
6	$1.62\pm$ .01	$.40\pm$ .01	$-.03\pm$ .01	$2.53\pm$ .07
7	$2.11\pm$ .02	$.33\pm$ .01	$-.18\pm$ .05	$2.65\pm$ .06
8	$2.57\pm$ .01	$.27\pm$ .01	$-.16\pm$ .03	$2.72\pm$ .07
9	$2.99\pm$ .02	$.23\pm$ .01	$-.1\pm$ .2	$3.0\pm$ .2
E_0 = 56230. GeV				
1	$-1.32\pm$ .13	$.88\pm$ .04	$.4\pm$ .2	$3.5\pm$ .4
2	$-.54\pm$ .02	$.67\pm$ .03	$.58\pm$ .06	$3.9\pm$ .2
3	$.00\pm$ .01	$.59\pm$ .02	$.50\pm$ .02	$3.63\pm$ .07
4	$.56\pm$ .01	$.52\pm$ .01	$.37\pm$ .03	$3.17\pm$ .04
5	$1.11\pm$ .01	$.46\pm$ .01	$.16\pm$ .03	$2.73\pm$ .05
6	$1.64\pm$ .02	$-.39\pm$ .01	$.05\pm$ .03	$2.58\pm$ .03
7	$2.14\pm$ .02	$.32\pm$ .01	$-.19\pm$ .03	$2.71\pm$ .05
8	$2.60\pm$ .02	$.27\pm$ .01	$-.15\pm$ .03	$2.8\pm$ .2
9	$3.02\pm$ .02	$.22\pm$ .01	$-.01\pm$ .08	$3.0\pm$ .2

Table A.1 — continued

Rad. bin	Average	Sigma	Skewness	Kurtosis
$E_0 = 100000.$ GeV				
1	$-1.39\pm$ .11	$.88\pm$ .02	$.3\pm$ .2	$3.8\pm$ .3
2	$-.55\pm$ .02	$.65\pm$ .03	$.57\pm$ .05	$4.0\pm$ .2
3	$.01\pm$ .01	$.58\pm$ .02	$.50\pm$ .02	$3.56\pm$ .07
4	$.57\pm$ .02	$.51\pm$ .01	$.34\pm$ .03	$3.12\pm$ .03
5	$1.12\pm$ .02	$.45\pm$ .01	$.14\pm$ .03	$2.77\pm$ .04
6	$1.65\pm$ .03	$-.39\pm$ .01	$.07\pm$ .03	$2.58\pm$ .04
7	$2.15\pm$ .02	$-.32\pm$ .01	$.18\pm$ .02	$2.7\pm$ .1
8	$2.61\pm$ .02	$.27\pm$ .00	$-.15\pm$ .03	$2.9\pm$ .1
9	$3.02\pm$ .02	$.22\pm$ .01	$-.01\pm$ .08	$3.0\pm$ .2

Table A.2

Central momenta for the distribution function of $\log(t/ns)$ for secondary e^+e^- produced at 2000 m a.s.l. by a γ primary, as obtained from the FLUKA stand-alone simulation. Primary γ, Sec. e^+e^-, $h_{\text{det}} = 2000$ m a.s.l.

Rad. bin	Average	Sigma	Skewness	Kurtosis
$E_0 = 562.$ GeV				
1	$-.45\pm$ .11	$1.13\pm$ .20	$-1.05\pm$ .6	$3.43\pm$ .6
2	$.03\pm$ .05	$.80\pm$ .15	$.1\pm$ .4	$2.4\pm$ .5
3	$.35\pm$ .24	$.64\pm$ .14	$.0\pm$ .6	$2.4\pm$ .6
4	$.65\pm$ .22	$.55\pm$ .15	$-.3\pm$ .5	$3.0\pm$ .5
5	$1.09\pm$ .18	$.42\pm$ .11	$-.1\pm$ .7	$3.1\pm$ .7
6	$1.40\pm$ .14	$.41\pm$ .13	$.0\pm$ .5	$3.8\pm$ .6
7	$1.85\pm$ .16	$.31\pm$ .11	$.2\pm$ .7	$3.8\pm$ .8
8	$2.38\pm$ .12	$.28\pm$ .05	$.0\pm$ .3	$2.8\pm$ .4
9	$2.78\pm$ .12	$.19\pm$ .05	$-.52\pm$ .3	$2.75\pm$ .4
$E_0 = 1000.$ GeV				
1	$-.39\pm$ .51	$.93\pm$ .20	$.0\pm$ .6	$2.2\pm$ .5
2	$.06\pm$ .27	$.70\pm$ .13	$-.2\pm$ .5	$2.2\pm$ .9
3	$.31\pm$ .20	$.63\pm$ .14	$.0\pm$ .5	$2.5\pm$ .6
4	$.73\pm$ .24	$.54\pm$ .14	$-.2\pm$ .6	$2.7\pm$ .8
5	$1.06\pm$ .19	$.42\pm$ .09	$-.1\pm$ .5	$3.1\pm$ .8
6	$1.44\pm$ .15	$.36\pm$ .09	$.1\pm$ .6	$3.4\pm$ 1.0
7	$1.83\pm$ .11	$.30\pm$ .07	$.0\pm$ .6	$2.6\pm$ .6
8	$2.36\pm$ .15	$.28\pm$ .06	$.2\pm$ .8	$3.1\pm$ 1.0
9	$2.83\pm$ .15	$.24\pm$ .06	$.91\pm$ .8	$4.10\pm$ 1.0
$E_0 = 1778.$ GeV				
1	$-.54\pm$ .38	$.95\pm$ .18	$-.2\pm$ .4	$2.5\pm$ .4
2	$.04\pm$ .33	$.73\pm$ .15	$-.2\pm$ .5	$2.5\pm$ .6
3	$.33\pm$ .25	$.61\pm$ .16	$-.2\pm$ .5	$2.5\pm$ .8
4	$.73\pm$ .19	$.51\pm$ .11	$-.3\pm$ .5	$2.5\pm$ .6
5	$1.05\pm$ .12	$.41\pm$ .07	$-.1\pm$ .5	$2.7\pm$ 1.0
6	$1.45\pm$ .10	$.34\pm$ .07	$-.1\pm$ .6	$3.3\pm$ 1.0
7	$1.88\pm$ .12	$.29\pm$ .07	$.0\pm$ .5	$2.9\pm$ .7
8	$2.35\pm$ .10	$.27\pm$ .06	$.3\pm$ .7	$2.9\pm$ .9
9	$2.91\pm$ .10	$.26\pm$ .06	$-.24\pm$ .8	$3.03\pm$ .9

Table A.2 — continued

Rad. bin	Average	Sigma	Skewness	Kurtosis
$E_0 = 3162.$ GeV				
1	$-.56\pm$ .40	$.84\pm$ .12	$-.1\pm$ .4	$2.4\pm$ .5
2	$-.09\pm$ .25	$.69\pm$ .14	$.1\pm$ .4	$2.8\pm$ .8
3	$.33\pm$ .15	$.60\pm$ .09	$.2\pm$ .3	$2.7\pm$ .4
4	$.73\pm$ .11	$.50\pm$ .06	$.0\pm$ .3	$2.5\pm$ .5
5	$1.07\pm$ .09	$.41\pm$ .05	$.0\pm$ .4	$2.8\pm$ .6
6	$1.44\pm$ .07	$.34\pm$ .06	$.2\pm$ .4	$3.0\pm$ .6
7	$1.90\pm$ .08	$.30\pm$ .06	$.0\pm$ .5	$3.5\pm$ 1.1
8	$2.39\pm$ .09	$.27\pm$ .07	$.2\pm$ .5	$2.6\pm$ .7
9	$2.88\pm$ .09	$.24\pm$ .07	$.05\pm$ .5	$2.34\pm$ .7
$E_0 = 5623.$ GeV				
1	$-.89\pm$ .33	$1.03\pm$ .19	$-.3\pm$ .4	$3.0\pm$ .9
2	$-.14\pm$ .20	$.67\pm$ .07	$.3\pm$ .3	$2.7\pm$ .4
3	$.32\pm$ .15	$.58\pm$ .07	$-.2\pm$ .3	$2.5\pm$ .3
4	$.75\pm$ .10	$.48\pm$ .05	$-.2\pm$ .3	$2.6\pm$ .4
5	$1.11\pm$ .08	$.40\pm$ .03	$-.1\pm$ .3	$2.7\pm$ .4
6	$1.48\pm$ .07	$.33\pm$ .03	$.0\pm$ .2	$3.2\pm$ .4
7	$1.92\pm$ .06	$.29\pm$ .03	$.0\pm$ .4	$3.0\pm$ .5
8	$2.40\pm$ .09	$.27\pm$ .05	$.1\pm$ .6	$3.2\pm$ .8
9	$2.90\pm$ .09	$.26\pm$ .05	$.04\pm$ .6	$2.26\pm$ .8
$E_0 = 10000.$ GeV				
1	$-.67\pm$ .31	$.96\pm$ .19	$-.3\pm$ .5	$3.0\pm$ .5
2	$-.13\pm$ .16	$.76\pm$ .10	$.0\pm$ .3	$2.5\pm$ .4
3	$.34\pm$ .07	$.56\pm$ .05	$.0\pm$ .1	$1.5\pm$ .2
4	$.74\pm$ .04	$.48\pm$ .03	$.0\pm$ .1	$2.7\pm$ .4
5	$1.08\pm$ .05	$.40\pm$ .03	$.0\pm$ .1	$2.5\pm$ .2
6	$1.44\pm$ .04	$.33\pm$ .02	$.1\pm$ .2	$2.9\pm$ .3
7	$1.90\pm$ .04	$.30\pm$ .03	$-.1\pm$ .3	$2.7\pm$ .4
8	$2.38\pm$ .05	$.26\pm$ .03	$.2\pm$ .3	$3.1\pm$ .5
9	$2.85\pm$ .09	$.25\pm$ .04	$.5\pm$ .3	$2.5\pm$ .4
$E_0 = 17780.$ GeV				
1	$-.61\pm$ .15	$.92\pm$ .13	$.1\pm$ .2	$2.5\pm$ .4
2	$-.05\pm$ .05	$.68\pm$ .04	$.1\pm$ .2	$2.3\pm$ .3
3	$.35\pm$ .05	$.57\pm$ .03	$.0\pm$ .1	$2.3\pm$ .1
4	$.73\pm$ .03	$.48\pm$ .02	$-.2\pm$ .1	$2.6\pm$ .2
5	$1.11\pm$ .03	$.41\pm$ .01	$-.06\pm$ .10	$2.6\pm$ .2
6	$1.47\pm$ .03	$.32\pm$ .02	$.0\pm$ .2	$3.0\pm$ .6
7	$1.92\pm$ .03	$.28\pm$ .02	$.2\pm$ .2	$3.0\pm$ .2
8	$2.43\pm$ .06	$.27\pm$ .02	$.2\pm$ .2	$3.1\pm$ .4
9	$2.88\pm$ .07	$.23\pm$ .04	$.1\pm$ .3	$2.2\pm$ .3
$E_0 = 31620.$ GeV				
1	$-.65\pm$ .19	$1.21\pm$ .06	$.11\pm$ .07	$5.0\pm$ .1
2	$-.05\pm$ .04	$.68\pm$ .02	$.2\pm$ .1	$2.2\pm$ .2
3	$.35\pm$ .03	$.56\pm$ .01	$-.01\pm$ .09	$2.1\pm$ .1
4	$.75\pm$ .02	$.49\pm$ .02	$-.16\pm$ .04	$2.4\pm$ .1
5	$1.10\pm$ .01	$.41\pm$ .01	$.01\pm$ .08	$2.9\pm$ .1
6	$1.47\pm$ .02	$.33\pm$ .01	$.15\pm$ .08	$2.9\pm$ .2
7	$1.92\pm$ .01	$.29\pm$ .01	$.1\pm$ .1	$3.1\pm$ .3
8	$2.39\pm$ .02	$.26\pm$ .01	$.0\pm$ .2	$2.7\pm$ .3
9	$2.88\pm$ .05	$.23\pm$ .02	$.3\pm$ .6	$3.0\pm$ .9

Table A.2 — continued

Rad. bin	Average	Sigma	Skewness	Kurtosis
$E_0 = 56230.$ GeV				
1	−.73± .11	.90± .06	−.1± .1	2.5± .3
2	−.09± .03	.68± .01	.12± .07	2.3± .1
3	.35± .02	.57± .01	.00± .04	2.45± .08
4	.75± .01	.47± .01	−.01± .06	2.53± .06
5	1.12± .02	.40± .01	−.04± .06	2.7± .1
6	1.49± .02	.33± .01	.04± .06	2.8± .1
7	1.94± .02	.29± .01	.1± .1	3.0± .2
8	2.43± .03	.25± .01	.1± .1	2.7± .4
9	2.92± .07	.25± .02	.2± .3	3.1± .6
$E_0 = 100000.$ GeV				
1	−.79± .11	.91± .01	−.02± .06	2.6± .2
2	−.08± .02	.66± .02	.14± .05	2.34± .06
3	.35± .02	.56± .02	.01± .03	2.48± .05
4	.77± .02	.47± .01	−.06± .04	2.60± .04
5	1.14± .03	.40± .01	−.01± .03	2.69± .04
6	1.51± .03	.33± .01	.09± .04	2.8± .2
7	1.96± .02	.29± .00	.11± .08	2.9± .2
8	2.45± .03	.27± .01	.1± .1	3.1± .2
9	2.93± .03	.22± .02	.1± .2	2.9± .4

Table A.3

Central momenta for the distribution function of $\log(t/ns)$ for secondary γ produced at 2000 m a.s.l. by a proton primary, as obtained from the FLUKA stand-alone simulation. Primary protons, Sec. γ, $h_{det} = 2000$ m a.s.l.

Rad. bin	Average	Sigma	Skewness	Kurtosis
$E_0 = 562.$ GeV				
1	.20± .40	.59± .14	1.12± .7	3.65± 1.4
2	.38± .34	.63± .13	.8± .6	3.3± 1.4
3	.55± .44	.64± .18	1.1± .9	3.9± 2.8
4	.62± .37	.64± .15	.8± .6	2.6± 1.1
5	.99± .28	.58± .14	.2± .6	2.7± 1.1
6	1.44± .25	.50± .13	.1± .7	2.6± 2.3
7	1.92± .21	.44± .12	−.1± .8	2.9± 2.4
8	2.36± .25	.41± .14	−.1± .9	3.1± 2.8
9	2.88± .34	.56± .19	.6± .9	5.6± 2.2
$E_0 = 1000.$ GeV				
1	−.25± .30	.59± .19	1.3± .9	4.5± 3.1
2	−.35± .45	.74± .14	.9± .5	3.2± 1.4
3	−.04± .33	.64± .15	1.1± .5	3.2± 1.2
4	.46± .36	.62± .11	.4± .5	2.6± 1.3
5	1.04± .27	.52± .13	.1± .5	2.9± 1.6
6	1.51± .22	.48± .11	−.2± .5	2.8± 1.4
7	1.99± .21	.44± .11	−.5± .7	3.7± 2.7
8	2.45± .24	.38± .12	−.2± .9	3.1± 3.1
9	2.91± .32	.54± .17	.5± .9	5.5± 2.4

Table A.3 — continued

Rad. bin	Average	Sigma	Skewness	Kurtosis
$E_0 = 1778.$ GeV				
1	.04± .24	.66± .07	.4± .9	3.0± 2.4
2	−.10± .40	.82± .18	.4± .6	2.8± .8
3	.12± .42	.72± .17	.8± .6	2.7± .9
4	.45± .32	.64± .11	.4± .5	2.7± .9
5	.97± .23	.54± .09	.1± .5	2.5± 2.2
6	1.49± .17	.47± .11	.0± .5	2.5± 1.9
7	1.99± .14	.40± .08	−.2± .8	2.7± 2.9
8	2.44± .19	.39± .11	−.2± .8	3.5± 2.8
9	2.93± .24	.50± .13	.5± .9	6.0± 2.6
$E_0 = 3162.$ GeV				
1	−.60± .44	.78± .18	1.2± .6	4.2± 1.5
2	−.53± .41	.78± .13	.6± .6	2.9± 1.4
3	−.09± .42	.71± .13	.3± .6	2.9± .8
4	.48± .26	.59± .12	.2± .4	3.1± .9
5	1.02± .18	.53± .10	.0± .4	2.7± .8
6	1.53± .13	.45± .07	−.1± .4	2.6± 1.7
7	2.03± .13	.40± .06	−.3± .6	3.1± 2.5
8	2.47± .17	.37± .07	−.3± .8	3.2± 2.9
9	2.95± .25	.50± .14	.5± .7	5.5± 2.1
$E_0 = 5623.$ GeV				
1	−.72± .48	.82± .25	.3± 1.0	2.7± 4.2
2	−.55± .63	.83± .17	.8± .6	3.1± .6
3	.03± .52	.65± .19	.5± .5	3.2± 30.3
4	.47± .23	.61± .09	.3± .4	2.8± 2.2
5	1.01± .12	.54± .10	.1± .3	2.8± .6
6	1.47± .13	.55± .10	−.5± .4	4.1± 1.4
7	2.03± .10	.40± .08	−.3± .4	3.1± 1.5
8	2.46± .15	.37± .09	−.3± .7	3.3± 2.7
9	2.92± .24	.49± .12	.3± .7	5.7± 2.0
$E_0 = 10000.$ GeV				
1	−.61± .39	.89± .20	.2± .5	2.4± .7
2	−.46± .36	.81± .16	.5± .4	2.8± .8
3	−.05± .24	.71± .08	.4± .3	3.1± .3
4	.49± .12	.60± .07	.3± .2	2.9± .3
5	1.02± .07	.52± .05	.1± .2	2.8± .7
6	1.54± .10	.45± .07	−.1± .2	2.8± .9
7	2.03± .07	−.39± .04	.2± .3	2.8± 1.5
8	2.49± .08	.34± .05	−.2± .6	3.2± 2.4
9	2.96± .11	.43± .07	.5± .6	5.3± 1.8
$E_0 = 17780.$ GeV				
1	−.62± .41	1.13± .13	.4± .3	5.8± .6
2	−.47± .33	.75± .04	.5± .3	2.7± .6
3	−.12± .17	.72± .07	.2± .2	3.4± .4
4	.48± .10	.58± .05	.2± .1	2.8± .3
5	1.06± .03	.49± .02	.13± .06	2.7± .3
6	1.57± .07	.43± .02	−.2± .2	2.7± .5
7	2.06± .05	.37± .02	−.2± .3	2.8± 1.0
8	2.51± .06	.33± .03	−.3± .4	3.4± 1.4
9	2.97± .03	.44± .03	.3± .5	5.9± 1.2

Table A.3 — continued

Rad. bin	Average	Sigma	Skewness	Kurtosis
E_0 = 31620. GeV				
1	−1.34± .52	.92± .07	.4± .4	3.3± .5
2	−.56± .24	.74± .08	.5± .2	3.6± .5
3	−.02± .12	.64± .06	.3± .2	3.3± .3
4	.53± .04	.56± .04	.25± .07	3.0± .2
5	1.07± .05	.49± .03	.0± .1	2.7± .3
6	1.59± .05	−.43± .02	.1± .2	2.7± .4
7	2.09± .05	.37± .03	−.3± .3	3.0± 1.1
8	2.53± .06	.33± .04	−.3± .5	3.4± 1.2
9	3.00± .08	.42± .03	.7± .4	5.5± .8
E_0 = 56230. GeV				
1	−1.29± .33	.88± .05	.5± .2	3.4± .3
2	−.58± .05	.70± .05	.51± .09	3.5± .2
3	−.03± .03	.62± .04	.46± .03	3.3± .2
4	.52± .04	.55± .02	.27± .06	3.0± .1
5	1.08± .03	.48± .02	.12± .05	2.7± .1
6	1.61± .03	.41± .01	−.1± .1	2.7± .3
7	2.10± .04	.36± .02	−.3± .1	2.9± .6
8	2.56± .04	.31± .02	−.2± .4	3.2± .8
9	3.05± .05	.43± .02	.7± .2	5.8± .5
E_0 = 100000. GeV				
1	−1.25± .11	.88± .05	.5± .1	3.3± .2
2	−.58± .08	.71± .06	.5± .1	3.7± .2
3	−.03± .04	.64± .03	.39± .09	3.4± .2
4	.52± .02	.55± .02	.28± .05	3.04± .07
5	1.08± .03	.48± .02	.08± .02	2.8± .1
6	1.61± .03	−.41± .01	.11± .05	2.7± .2
7	2.10± .02	.35± .01	−.3± .1	2.9± .6
8	2.56± .03	.31± .02	−.2± .2	3.2± .6
9	3.02± .04	.40± .02	.6± .2	5.1± .6

Table A.4

Central momenta for the distribution function of $\log(t/ns)$ for secondary $e^+ e^-$ produced at 2000 m a.s.l. by a proton primary, as obtained from the FLUKA stand-alone simulation Primary protons, Sec. $e^+ e^-$, h_{det} = 2000 m a.s.l.

Rad. bin	Average	Sigma	Skewness	Kurtosis
E_0 = 562. GeV				
1	.26± .30	.43± .10	.37± .7	1.90± .10
2	.49± .27	.63± .11	.85± .6	3.74± .8
3	.57± .27	.59± .11	.2± .6	2.2± .8
4	.66± .26	.54± .11	.2± .7	2.1± 1.4
5	.93± .28	.50± .12	−.2± .8	3.4± 2.4
6	1.30± .23	.43± .12	.0± .7	2.9± 1.7
7	1.72± .28	.43± .19	.1± 1.0	3.5± 1.8
8	2.23± .36	.44± .20	.4± 1.0	3.5± 1.5
9	2.74± .34	.60± .27	.3± 1.0	5.8± 5.8

Table A.4 — continued

Rad. bin	Average	Sigma	Skewness	Kurtosis
E_0 = 1000. GeV				
1	.17± .29	.69± .19	.2± .5	2.2± .6
2	−.03± .36	.79± .15	.2± .5	2.1± .8
3	.17± .25	.68± .11	.2± .5	2.3± .6
4	.60± .17	.54± .11	−.2± .6	2.4± .8
5	1.02± .26	.47± .12	−.1± .6	3.3± 1.0
6	1.34± .24	.43± .12	−.1± .8	3.6± 3.1
7	1.81± .28	.58± .17	−.2± 1.1	5.8± 3.7
8	2.32± .34	.56± .19	1.0± 1.0	5.9± 2.1
9	2.77± .37	.50± .18	.2± .9	3.2± 1.9
E_0 = 1778. GeV				
1	.42± .40	.62± .20	.54± .5	2.50± .4
2	.15± .40	.78± .19	−.2± .4	2.3± .3
3	.28± .21	.69± .13	.0± .5	2.4± .7
4	.56± .18	.56± .13	−.1± .6	2.0± .8
5	.95± .18	.46± .11	.0± .7	2.8± 1.6
6	1.33± .19	.41± .10	.2± .7	3.2± 1.9
7	1.81± .20	.36± .11	.3± .8	3.1± 1.9
8	2.31± .29	.51± .16	.2± 1.0	4.8± 2.3
9	2.86± .24	.55± .20	1.1± .9	5.1± 1.8
E_0 = 3162. GeV				
1	−.32± .30	.77± .20	.1± .5	2.2± .8
2	−.14± .31	.80± .14	−.2± .4	2.7± .9
3	.20± .23	.67± .11	−.2± .4	2.5± .5
4	.63± .18	.53± .09	−.1± .4	2.8± 1.0
5	1.01± .18	.47± .11	−.2± .4	2.9± .6
6	1.36± .15	.40± .09	−.2± .8	3.3± 3.8
7	1.82± .19	.37± .13	−.1± 1.0	3.1± 3.6
8	2.32± .26	.42± .18	.3± .8	3.7± 2.1
9	2.88± .37	.58± .20	.0± .7	5.5± 1.5
E_0 = 5623. GeV				
1	−.31± .27	.85± .20	−.1± .6	2.4± 1.0
2	−.20± .46	.86± .16	−.1± .4	2.5± .6
3	.31± .24	.63± .14	−.1± .6	2.4± 1.1
4	.59± .26	.55± .11	−.4± .4	2.9± .5
5	1.00± .14	.47± .10	−.2± .5	2.8± 2.1
6	1.29± .15	.50± .11	−.5± .8	4.7± 2.4
7	1.83± .13	.40± .11	.0± .5	3.8± 1.5
8	2.34± .20	.41± .16	.4± .9	4.1± 2.1
9	2.83± .35	.65± .19	.5± .9	4.3± 1.6
E_0 = 10000. GeV				
1	−.16± .32	.83± .19	−.3± .4	2.7± .7
2	−.15± .28	.79± .15	−.2± .4	1.8± .5
3	.23± .22	.68± .10	−.3± .3	2.3± .6
4	.63± .12	.55± .08	−.2± .3	2.7± .3
5	1.01± .10	.46± .06	−.2± .5	2.9± 1.4
6	1.38± .13	.39± .07	−.1± .8	3.2± 4.4
7	1.81± .10	.37± .07	.1± .9	3.3± 4.1
8	2.33± .14	.38± .09	.2± .9	3.4± 2.6
9	2.88± .22	.56± .15	.5± .7	5.7± 1.6

Table A.4 — continued

Rad. bin	Average	Sigma	Skewness	Kurtosis
E_0 = 17780. GeV				
1	$-.22\pm$ .42	$.82\pm$ .14	$-.1\pm$ .3	2.7$\pm$ .3
2	$-.12\pm$ .26	$.78\pm$ .08	$-.2\pm$ .5	3.4$\pm$ 1.1
3	$.21\pm$ .09	$.67\pm$ .06	$-.1\pm$ .2	2.9$\pm$ .4
4	$.63\pm$ .07	$.53\pm$ .05	$-.24\pm$ .10	2.7$\pm$ .3
5	1.06$\pm$ .04	$.43\pm$ .04	$-.1\pm$ .2	2.8$\pm$ .5
6	1.40$\pm$ .06	$.37\pm$ .03	$.0\pm$ .5	2.9$\pm$ 3.5
7	1.85$\pm$ .06	$.34\pm$ .03	$.1\pm$ 1.3	3.4$\pm$ 5.8
8	2.34$\pm$ .14	$.38\pm$ .09	$.1\pm$ .8	3.8$\pm$ 2.1
9	2.93$\pm$ .13	$.50\pm$ .08	1.1$\pm$ .5	4.5$\pm$ 1.5
E_0 = 31620. GeV				
1	$-.78\pm$ .43	$.91\pm$ .13	$.0\pm$ .3	2.0$\pm$ .5
2	$-.14\pm$ .21	$.71\pm$ .08	$-.1\pm$ .2	2.6$\pm$ .3
3	$.29\pm$ .12	$.62\pm$ .06	$-.2\pm$ .3	2.8$\pm$ .8
4	$.70\pm$ .05	$.52\pm$ .03	$-.14\pm$ .10	2.7$\pm$ .3
5	1.07$\pm$ .06	$.44\pm$ .03	$-.2\pm$ .1	3.0$\pm$ .6
6	1.43$\pm$ .06	$.37\pm$ .03	$-.1\pm$ .3	3.0$\pm$ 1.2
7	1.87$\pm$ .05	$.35\pm$ .03	$.0\pm$ .9	3.2$\pm$ 3.4
8	2.38$\pm$ .08	$.38\pm$ .07	$.3\pm$ .8	4.2$\pm$ 2.3
9	2.88$\pm$ .15	$.47\pm$ .08	$.5\pm$ .5	5.5$\pm$ 1.0
E_0 = 56230. GeV				
1	$-.73\pm$ .23	$.90\pm$ .06	$.1\pm$ .2	1.9$\pm$ .3
2	$-.17\pm$ .02	$.70\pm$ .04	$.0\pm$ .1	2.5$\pm$ .3
3	$.29\pm$ .05	$.61\pm$ .03	$-.02\pm$ .07	2.29$\pm$ .09
4	$.69\pm$ .04	$.51\pm$ .02	$-.15\pm$ .08	2.4$\pm$ .4
5	1.08$\pm$ .03	$.43\pm$ .02	$-.1\pm$ .1	2.7$\pm$ .4
6	1.45$\pm$ .03	$.36\pm$ .02	$.0\pm$ .3	3.0$\pm$ 1.9
7	1.92$\pm$ .04	$.34\pm$ .02	$.2\pm$ .3	3.3$\pm$ 2.1
8	2.44$\pm$ .06	$.44\pm$ .04	$.3\pm$ .2	4.9$\pm$ 1.0
9	2.98$\pm$ .09	$.51\pm$ .04	$.5\pm$ .3	6.1$\pm$ .5
E_0 = 100000. GeV				
1	$-.72\pm$ .14	$.90\pm$ .03	$.1\pm$ .2	1.9$\pm$ .2
2	$-.14\pm$ .08	$.70\pm$ .06	$.0\pm$ .1	2.3$\pm$ .1
3	$.29\pm$ .04	$.61\pm$ .03	$-.13\pm$ .07	2.6$\pm$ .1
4	$.69\pm$ .02	$.52\pm$ .02	$-.14\pm$ .04	2.68$\pm$ .09
5	1.08$\pm$ .03	$.43\pm$ .01	$-.08\pm$ .06	2.8$\pm$ .2
6	1.45$\pm$ .03	$.36\pm$ .01	$.0\pm$ .2	3.0$\pm$ 1.9
7	1.90$\pm$ .03	$.34\pm$ .02	$.0\pm$ .4	3.2$\pm$ 2.1
8	2.42$\pm$ .04	$.37\pm$ .03	$.4\pm$ .2	4.0$\pm$ 1.2
9	2.96$\pm$ .07	$.51\pm$ .05	$.6\pm$ .3	5.7$\pm$ 1.1

References

[1] B. D'Ettorre, G. Di Sciascio, Astropart. Phys. 2 (1994) 199.

[2] G. Agnetta et al., Astropart. Phys. 6 (1997) 301.

[3] M. Ambrosio et al., Astroparticle Phys. 7 (1997) 329.

[4] The EAS-TOP Collaboration, Nucl. Instr. Meth. A 336 (1993) 310.

[5] P. Bassi, G. Clark, B. Rossi, Phys. Rev. 92 (1953) 441.

[6] J. Linsley, L. Scarsi, B. Rossi, Phys. Rev. Lett. 6 (1961) 485.

[7] J. Linsley, L. Scarsi, Phys. Rev. 128 (1962) 2384.

[8] A.A. Watson, J.G. Wilson, J. Pjys. A 7 (1976) 1199.

[9] C.P. Woidneck, E. Böhm, J. Phys. A 8 (1975) 997.

[10] J. Linsley, J. Phys. G 12 (1986) 51.

[11] A.J. Baxter, A.A. Watson, J.G. Wilson, Proc. 9th ICRC, London, England, Vol. 2, p. 724.

[12] G.B. Khristyansen et al., Proc. 21th ICRC, Adelaide, Australia, Vol. 9 (1990) p. 150.

[13] P.K.F. Grieder, Acta Phys. Suppl. Acad. Sci. Hung. 29 (1970) 563, 569.

[14] H.E. Dixon et al., Proc. Roy. Soc. London A 339 (1974) 133.

[15] K.E. Turver, Proc. 14th ICRC, Munich, Germany, Vol. 8 (1975) p. 2581.

[16] T.K. Gaisser et al., Rev. Mod. Phys. 50 (1978) 859.

[17] Y. Mizumoto et al., Proc. 16th ICRC, Kyoto, Japan, Vol. 9 (1979) p. 116.

[18] E.J. de Villiers et al., J. Phys. G 12 (1986) 547.

[19] S. Mikocki et al., J. Phys. G 13 (1987) L85.

[20] T.V. Danilova et al., Proc. 20th ICRC, La Jolla, USA, Vol. 6 (1987) p. 43.

[21] S. Mikocki et al., J. Phys. G 17 (1991) 1303.

[22] A.V. Plyasheshnikov, Proc. 22nd ICRC, Dublin, Ireland, Vol. 1 (1991) p. 488.

[23] H. Rebel et al., J. Phys. G. 21 (1995) 451.

[24] M. Ambrosio et al., Proc. 1996 Vulcano Workshop on: Frontier Objects in Astrophysics and Particle Physics, F. Giovannelli, G. Mannocchi, eds. (SIF Bologna, Italy, 1996) p. 429;
M. Ambrosio et al., Nucl. Phys. B (Proc. Suppl.) 52B (1997) 234.

[25] J.N. Capdevielle et al., Report KfK 4998, Kernforschungszentrum Karlsruhe (1992);
J. Knapp, D. Heck, Report 5196B, Kernforschungszentrum Karlsruhe, update versions (1993).

[26] V. Patera et al., Nucl. Instr. Meth. A 356 (1995) 514.

[27] S. Roesler, W. Heinrich, H. Schraube, Radiation Research 149 (1998) 87.

[28] G. Battistoni et al., A new calculation of atmospheric neutrino flux: the FLUKA approach, in: Proc. TAUP conference 1997, Laboratory Nazionali del Gran Sasso (Italy) (1997), proceedings in press.

[29] A. Fassó et al., FLUKA: present status and future developments, in: Proc. IV Int. Conf. on Calorimetry in High Energy Physics, La Biodola (Italy) (World Scientific, Singapore, 1993) p. 493.

[30] R. Brun et al., CERN GEANT 3 User's Guide, DD/EE/84-1 (1987).

[31] A. Fassó et al., Proc. MC93 Int. Conf. on Monte Carlo Simulation in High-Energy and Nuclear Physics, Tallahassee, USA 1993, P. Dragovitsch, S.L. Linn, M. Burbank, eds. (World Scientific, Singapore, 1994) p. 277.

[32] A. Ferrari et al., An improved multiple scattering model for charged particle transport, Nucl. Instr. Meth. B 71 (1992) 412.

[33] T.K.Gaisser, Cosmic Rays and Particle Physics (Cambridge Univ. Press, Cambridge, 1990) p. 34.

[34] W.T. Eadie, D. Drijard, F.E. James, M. Roos, B. Sadoulet, Statistical Methods in Experimental Physics (North-Holland, Amsterdam, 1971) p. 80.

[35] T.V. Danilova et al., J. Phys. G 20 (1994) 961.

[36] A. Stuart, J.K. Ord, Kendall's Advanced Theory of Statistics [originally by Sir M. Kendall], Vol. 1, (Charles Griffin & Co., London, 1987) ch. 6.

[37] A. Ferrari et al., Z. Phys. C 70 (1995) 413.

[38] A. Ferrari et al., Z. Phys. C 71 (1996) 75.

[39] J. Ranft, Phys. Rev. D 51 (1995) 64.

[40] A. Di Sciascio et al., Astropart. Phys. 6 (1997) 313.

[41] For a recent list of MACRO authors, see M. Ambrosio et al., Phys. Rev. D 56 (1997) 1407, 1418.